4.7 THz asymmetric beam multiplexer for GUSTO

BEHNAM MIRZAEI,[1,2,7] (iD) YUNER GAN,[2,3] (iD) MATVEY FINKEL,[2] CHRISTOPHER GROPPI,[4] ABRAM YOUNG,[5] CHRISTOPHER WALKER,[5] QING HU,[6] AND JIAN-RONG GAO[1,2,8]

[1]*Optics Research Group, Department of Imaging Physics, Delft University of Technology, Van der Waalsweg 8, 2628 CH, Delft, The Netherlands*
[2]*SRON Netherlands Institute for Space Research, Niels Bohrweg 4, 2333 CA Leiden and Landleven 12, 9747 AD Groningen, The Netherlands*
[3]*Kapteyn Astronomical Institute, University of Groningen, 9747 AD, Groningen, The Netherlands*
[4]*School of Earth and Space Exploration, Arizona State University, AZ 85287, USA*
[5]*Steward Observatory, University of Arizona, 933 N Cherry Ave, Tucson, AZ 85719, USA*
[6]*Department of Electrical Engineering and Computer Science and Research Laboratory of Electronics, Massachusetts Institute of Technology, Cambridge, Massachusetts 02139, USA*
[7]*b.mirzaei@tudelft.nl*
[8]*j.r.gao@sron.nl*

Abstract: A full demonstration of the Fourier phase grating used as 4.7 THz local oscillator (LO) multiplexer for Galactic/Extragalactic ULDB Spectroscopic Terahertz Observatory (GUSTO) is presented in this paper, including its design, modeling, tolerance analysis, and experimental characterizations of the angular and intensity distributions among 2 × 4 output beams and the power efficiency. A quantum cascade laser (QCL) is used to generate the input beam for evaluation of the grating performance in its all relevant aspects with an accuracy level never reported before, where good agreements with modeling results are found. This is the first asymmetric-profile grating fully modelled and characterized at a THz frequency, that further confirms the versatility of this technology for providing an intermediate optical element for feeding multiple array detectors with a single radiation source at such a scientifically interesting frequency regime.

1. Introduction

Galactic/Extragalactic ULDB Spectroscopic Terahertz Observatory (GUSTO) is a NASA supported balloon borne astronomical observatory for studying the life-cycle in the interstellar medium and beyond. It will detect the transition lines of nitrogen, carbon and oxygen at frequencies of 1.4, 1.9 and 4.7 THz (called bands 1, 2 and 3 respectively). High spectral resolution spectroscopy is provided by the heterodyne detection technique that is employed for all three frequency bands. In this technique the THz celestial signal is down-converted to GHz range when it is mixed with a locally generated signal (LO). This is done by the state-of-the-art sensitive superconducting hot electron bolometer (HEB) mixers in GUSTO. Each band has an array of 8 (2 × 4) mixers for increasing the mapping speed and the observing efficiency. These arrays at two lower frequency bands i.e. 1.4 and 1.9 THz are optically pumped with LOs generated by an array of frequency multiplied sources [1]. However, this technology is not yet available at 4.7 THz because of the upscaled machining difficulties for shorter wavelengths. At such a high frequency QCLs [2] are the only LO-applicable radiation source, the outcome of more than two decades of efforts on improving both their gain medium [3], where the optical inter-subband transitions of electrons happen and their waveguide structure to couple their radiation to the free space [4].

In GUSTO's band-3 a unidirectional 3'rd order distributed feedback (DFB) QCL [5] will be used as the LO. The radiation from such a QCL is directed through an optical system for properly coupling to the array's 8 mixers equidistantly distributed in a 2 × 4 rectangular pattern. The latter can be done in the most efficient way using a Fourier phase grating not only for this frequency range [6,7] but also at lower THz frequencies [8]. In this paper we report the demonstration of such a 4.7 THz phase grating as the LO multiplexer with an unprecedented asymmetric profile, which allows for meeting the specific requirement of the 8 beams of GUSTO. We also apply a novel high power QCL source at 4.7 THz, which in combination with our experimental arrangement allows for the characterization of the angular distribution of the output beams, the efficiency and the power uniformity in a high accuracy. Both the idea to use an asymmetric grating profile at such a high frequency and the accurate experimental characterization have never been reported in the literature before.

2. Phase grating design

A phase grating is formed by repetition of a unit-cell, which is engineered to diffract the input beam into required directions or modes. While the surface topology of the unit-cell determines the power distribution among different diffraction modes, its size determines the angular distances between them. The design of the LO coupling optical system of GUSTO's band-3 requires a reflective grating to multiplex an Gaussian-like incoming beam of 2.95 mm radius with 15 ° angle of incidence to 8 (2 × 4) beams with equal angular distances of 1.83 °. The angles of incidence (α) and mth diffraction order (β) are related to each other through a basic formula i.e. $\sin \beta = \sin \alpha + m\lambda/\Lambda$, where λ is the wavelength, m is the diffraction order and Λ is the grating periodicity. The latter is the same as the unit-cell size. The conventional way of symmetric designation of diffraction orders ($\pm 1, 2, \dots$) requires a unit-cell size of more than 4 mm. Considering the fact that for the grating to function at least 2 unit-cells should be illuminated, a symmetric structure is not applicable since the input beam diameter is ∼ 6mm. The only way to accommodate the required function is then applying the asymmetrically distributed consecutive orders [9]. For this we chose the orders (0,+1) and (−2,−1,0,+1) for the beam to be multiplexed in orthogonal directions. This is the first time that the asymmetric approach is taken for beam multiplexing at THz.

We use MATLAB to generate the grating surface profile with the same method as described in [10]. However, in order to derive an asymmetric profile we apply both sine and cosine components in the expansion of the phase modulation function, where for each of which, we calculate 5 Fourier coefficients. COMSOL is then used to characterize the performance of the grating, when it is illuminated with a Gaussian beam at its waist with 15 ° incidence angle. The designed surface topology of a unit-cell is shown in Fig. 1(a) in 3D, where its asymmetric feature can be seen. The cross-section 2D profiles in orthogonal directions are also shown in this figure (b) and (c), where one multiplexes the beam by 2 and the other by 4. The grating surface is made by superimposing these two profiles over a certain rectangular area, whose side-lengths define the angular separation of the output beams in both directions. The arrow schematics help to understand how the incident beam illuminates the grating and the output beams are diffracted from.
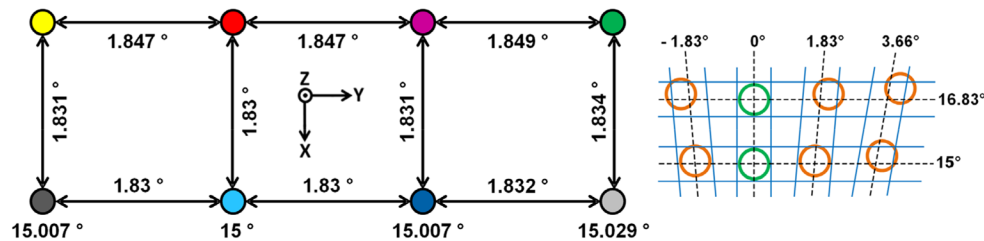
The angular distances between the output beams should be considered altogether when the side-lengths of a grating unit-cell is being determined, for which the abovementioned formula is not fully applicable since the incoming beam is simultaneously multiplexed by two superimposed profiles. Here we use COMSOL to derive the optimized side-lengths for having the closest angular distances to 1.83°, where we find the lengths of 2.057 mm and 2.048 mm for the 1 × 2 and 1 × 4 multiplexing profiles, respectively. The resulted angular pattern is shown in Fig. 2, in which all the angular distances amongst the beams (with similar colors as to Fig. 1) in X and Y directions are given. Moreover, the distances from the normal in the X direction
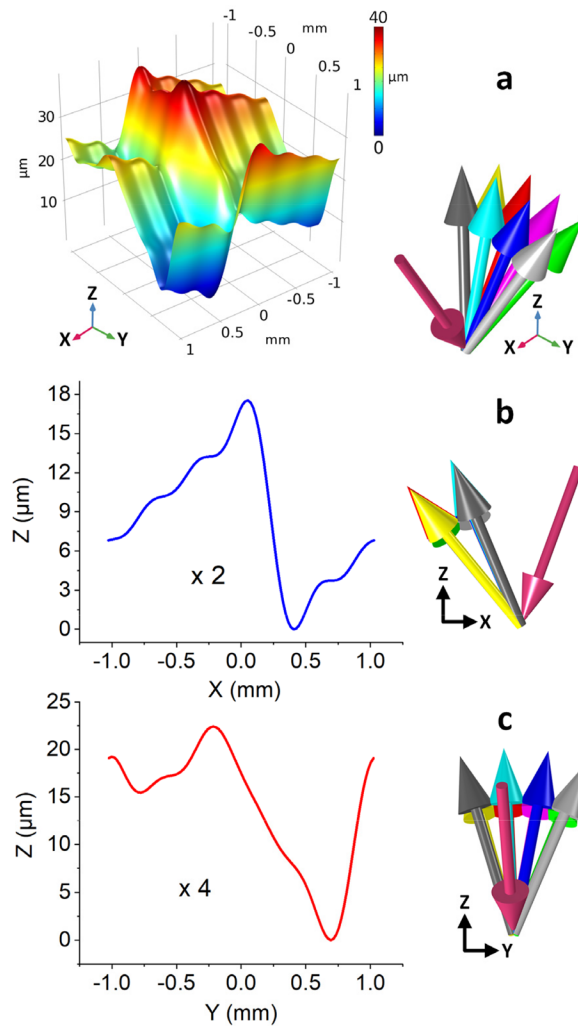
Fig. 1. 3D topology of the grating surface (a), and its 2D cross-section profiles (b, c). Arrow schematics show the incident beam and the diffracted beams in corresponding coordinates to their adjacent profiles.

(incident beam plain) are given for the first row beams on their bottoms, which is 15 ° for the (0,0) diffraction order (30 ° from the incident beam) and different for the others. These angles give a clear imagination of the beam's distribution scheme. We show an exaggerated view of such distribution on the right side of this figure to help reader's perception, which indicates that the (0,0) order is a flat mirror image of the incident beam flowing in the same plane (0 ° distance in Y direction) with the same distance from the normal (15 °). The maximum deviation occurs for the beam on the top right corner, which is 0.033 ° and 0.036 ° in X and Y directions respectively.

The designed surface topology is expected to provide an efficiency of ∼ 70%, which is the ratio between the summed power over the targeted diffraction orders to the power of the incoming beam. The other important characteristic is the uniformity in the power distribution among the output beams. This is important for an array of similar mixers, DC-biased on the same optimal operating point. If the LO coupling deviates from the optimum for any of mixers its heterodyne sensitivity degrades accordingly. For this grating we expect a non-uniformity of

Fig. 2. Angular distribution of the output beams. Angular distances are written on the arrows between the beams. The angles to the normal in X direction (incident beam plain) are quoted for the first row beams on their bottoms. A distribution view with exaggerated angular deviations is given on the right side.

13% defined as the $(P_{max}-P_{min})/P_{average}$, where P_{max} and P_{min} are the maximum and minimum powers respectively, and $P_{average}$ is the averaged distributed power among all the output beams. The detailed power distribution scheme would be later shown and compared to the measurement results in this paper. To estimate the effect of such non-uniformity on the sensitivity of the mixer array we use a set of experimental I-V curves measured for an HEB with different levels of the LO pumping powers [11]. We find that the averaged addition to the receiver noise temperature (T_N) is 1.5% if the designed grating is applied. The reason for averaging is that in the observation each point in sky is scanned by all the array pixels and the final result is the average of the individual ones. The latter defines the averaged array sensitivity.

3. Manufactured grating and surface deviation analysis

The acquired grating surface, which is machined on an aluminum block by micro-milling, has random deviations from the design not in a systematic way, whose influence is difficult to derive by modelling. However, in order to understand the order of the effect of a profile deviation on the grating performance we apply surface modifications to our design by adding a 1 mm period sine-surface with different amplitudes to the grating profile. Figure 3 shows the added surface and the grating profile. We think this approach covers the deviation caused by machining. i.e. it gives bigger effects than the actual derived profile and therefore can be taken as a measure for the surface tolerance.

We find that the application of such surface perturbations causes negligible change in the grating efficiency. However, it degrades the uniformity of the power distribution and consequently the receiver sensitivity as explained in the previous section. Results are summarized in Table 1 for different amplitudes of the added sine-wave surface.

The grating is manufactured at Arizona State University using a CNC micro-milling machine. It has 12 by 12 unit-cells covering a surface area of ∼ 25 mm². An optical micrograph of two unit-cells of the manufactured grating together with a simulated image of the same area projected with a similar light are shown in Fig. 4(a) and (b) respectively. Since the surface of the grating has a large minimum radius of curvature (∼ 1.4 mm) or in other words shallow features distributed over long lengths it is difficult to show its fine structures clearly by imaging. However, one can see the main surface height transitions followed by the shadows on this figure. To better address the imaged area a larger simulated surface with highly magnified structures is shown in c, where the plane is slightly rotated around the Y axis for a better 3D representation, and the imaged area is indicated by a white rectangle.

The height data of the machined surface is acquired using a 3D microscope and compared to the designed profile, where deviations less than 1 μm are found. The design and manufactured cross-section profiles of a unit-cell in orthogonal directions are shown in Fig. 5 together with
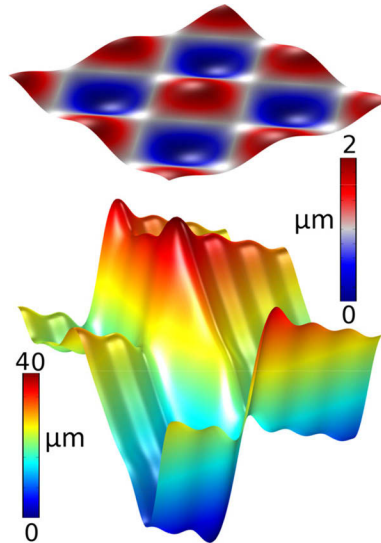
**Fig. 3.** The added sine-wave surface (1 µm amplitude) to the grating profile for estimation of the effect of the machining imperfections on the grating performance.

**Table 1. Consequences of the Grating Surface Deviation[a]**

Amplitude	Non -uniformity	Averaged addition to TN
1 µm	25%	5%
0.7 µm	21%	4%
0.6 µm	19%	3.5%
0.5 µm	17%	3%
0.4 µm	15%	2.5%
0.2 µm	14%	2%
Ideal	13%	NA

[a]The non-uniformities and averaged additions to the receiver noise temperature (T_N), when 1 mm period sine-wave perturbations with different amplitudes are applied to the grating profile.
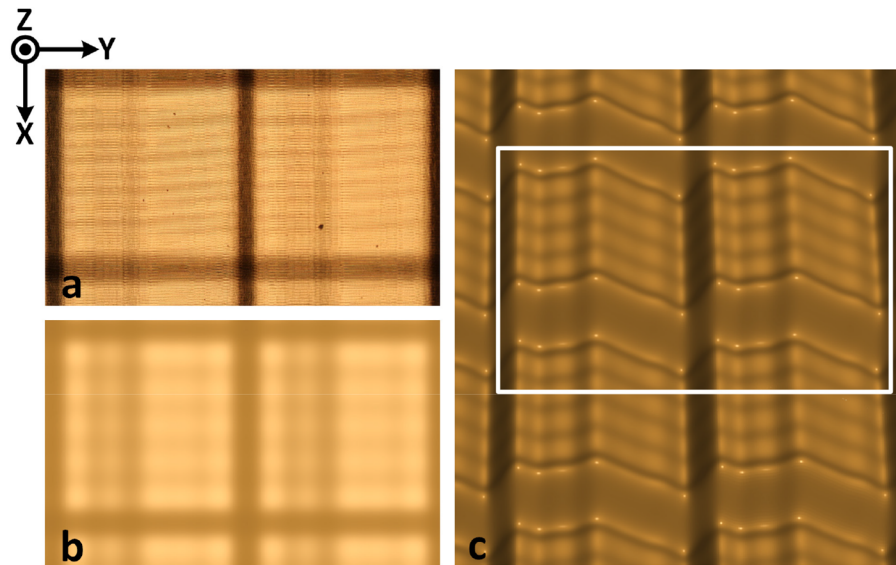
Fig. 4. (a), (b) Optical micrograph of two unit cells of the manufactured grating on an aluminum block and simulated image of the same area with a similar light projection, respectively. The coordinate system corresponds to the one used in Fig. 1. (c) simulated image of a larger surface, where the features are highly magnified and the plane is slightly rotated around the Y axis to give the reader a clear perception of the imaged area indicated by the white rectangle.

their height differences or deviations. With this we expect a reduction in the averaged array sensitivity by less than 5% (Table 1).
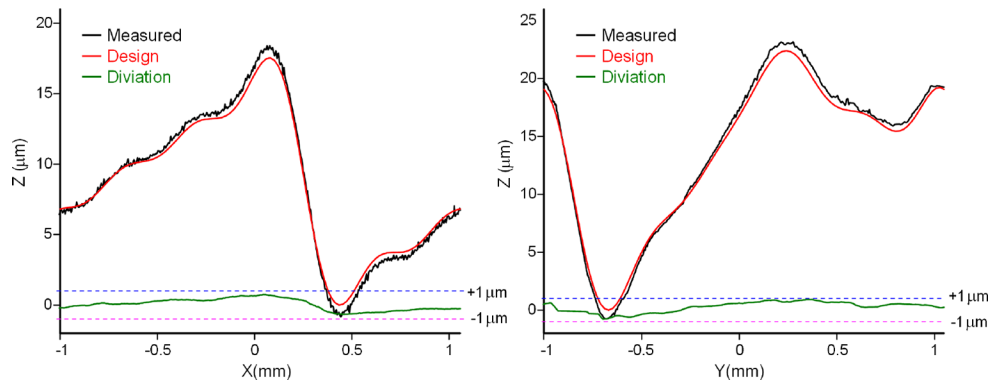

Fig. 5. Designed and measured cross-section profiles of the grating in orthogonal directions and their deviations.

4.   Measurement setup and results

4.1.   4.7 THz radiation source

We use a unidirectional 4.7 THz QCL [5] developed by MIT with an exceptional high output power for characterization of the manufactured grating. The QCL chip on a Cu plate is shown in the inset of the Fig. 6(a). We mount it in a pulse-tube cryo-cooler, where the THz radiation

transmits through an UHMW-HDPE window. We scan the raw beam pattern of this laser at a distance of ∼ 50 mm using a pyro-electric detector mounted on a 2D translational stage. The acquired beam is shown in Fig. 6(b). The orientation relation between the laser chip and the scanned beam pattern is indicated using a common coordinate system shown on both in Fig. 6. We also measure its spectrum using a Fourier transform spectrometer and the result is shown in Fig. 6(a), where its single-mode feature peaking at ∼ 4.715 THz can be seen. This frequency is slightly lower (0.6%) than the one the grating is designed for i.e. 4.745 THz, that causes negligible effect on the grating performance. The output power of this laser is ∼ 5 mW, determined using a Thomas Keating power meter.
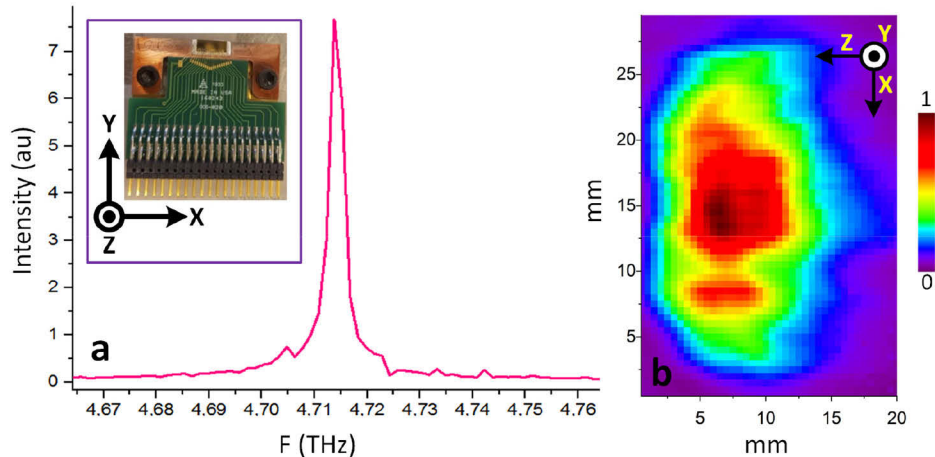

Fig. 6. (a) Single-emission mode spectrum of the used QCL, where the line-width is limited by the resolution of the Fourier transform spectrometer. The inset is a photo of the QCL chip on a Cu plate. (b) The beam pattern scanned at a distance of ∼ 50 mm from the laser chip. The coordinates on both sides are to indicate the orientation relation between the laser chip and the beam pattern.

4.2. Measurement setup

As mentioned before, we scan the beams using a pyro-electric detector mounted on a 2D translational stage. We mount the translational stage on a robust rail-slider to be able to move the stage back and forth (in the Z direction, normal to the scanning plane, X-Y). We need this to finely identify the beam traveling direction since the angular accuracy is crucial in this measurement. We find the uncertainty of the detector position on the scanning plane caused by the rail-slider to be less than ± 15 μm, by several scanning-sliding-scanning rounds of the beam on the same plane. This leaves a negligible uncertainty in the angle measurements since the distances that we take between our scanning planes are in the order of couple of centimeters.

The first step of the experiment is preparing a suitable input beam with a right incident angle to the grating. Since the output beams would have small angular distances from each other, in order to have them resolved in a reasonable distance from the grating, a highly collimated beam with a small size should be made as the input. To do so we use a 60 mm focal length HDPE lens to collimate the QCL beam, which undergoes spatial filtering by two 6 mm diameter iris apertures before and after the lens. There is a tilt adjustable flat mirror between the lens and the aperture 2 for vertically straightening the beam direction. A schematic of the setup is shown in Fig. 7.

We scan the beam in several planes with different distances from the aperture 2 until we see a consistent beam shape. There would be in the far-field regime, where the beam is in its final form and we can keep track of it to identify its traveling direction. We find this range starting at ∼ 20
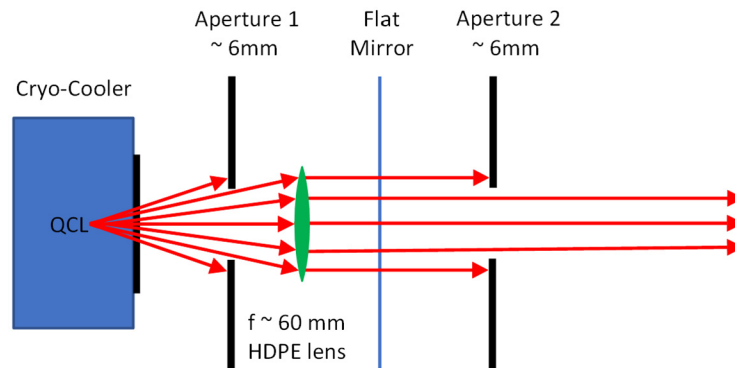
Fig. 7. The optical setup for providing the input beam to the grating

cm away from the aperture 2. In this range we keep scanning the beam in 3 different planes with a 40 mm interval, while optimizing our sliding direction (Z) until we find the scanned beams straight along the rail. Thereafter, we mark the rail direction as the direction of the input beam, based on which the grating angle should adjusted.

To position the grating with a correct angle with respect to the incident beam (15 °) we take advantage of the (0,0) diffraction order mode, which reflects off the grating similar to a flat mirror. With this we expect to have 30 ° distance between the incident beam and the (0,0) mode. Therefore, before placing the grating we make an angle of 30 ° to the recorded direction of the incident beam. The rail-slider then is placed in parallel to the latter. Here we scan and find the (0,0) mode and then optimize the grating angle till we see this mode travelling along the rail direction. In this step the setup is completed and the output beams can be measured. For each step of finding and recording the traveling direction we assume an error of 0.1 ° leading to a total of 0.3 ° (3 steps: finding the incident angle, adding 30 ° distance to it, and positioning the rail) uncertainty in the incident angle. This causes a negligible difference in the angular separation of the beams (< 0.01 °). By performing COMSOL simulation we find less than 1% effect on the grating efficiency and a maximum addition of 1.5% to the power distribution non-uniformity (ideally, 13%) caused by such uncertainty.

4.3. Results

We place the grating at a distance of ∼ 22 cm from the aperture 2 and scan the output beams at a distance of ∼ 34 cm from the grating. We observe 8 diffracted beams in the expected distribution. However, the shape of each beam does not resemble the incident beam. We explain this issue as follows. The input beam to the grating has an 8 mm diameter with tails extended to the edge of the grating active surface, which causes truncation and consequently the appearance of side-lobes around all the beams in the far-field diffraction pattern. The side-lobes of each diffracted beam can then interfere with its adjacent beams and their side-lobes and vice-versa, that lead to changes in their shapes. Although we cannot use this output for calculation of the grating efficiency and power uniformity we can still use it to determine the angular distances between the beams since this issue does not influence their travelling direction.

We measure the direction of each beam individually by scanning it at three different planes. We first fit the scanned beams to Gaussian distributions and then linear-least-squares fit the three acquired Gaussian center points to obtain the beam direction. The results of such measurements are shown in Fig. 8(b) besides the expected angular distances from modelling in Fig. 8(a). There the beams are numbered for easier tracking in the text, where the (0,0) order mode is indicated with number 3. The top and bottom numbers written on each arrow are the horizontal and vertical

angles between the beams at its two ends respectively. We quote uncertainties inside prentices caused by three major contributors i.e. the unlocking-sliding-locking of the stage mounted on the rail-slider and the standard errors in the Gaussian and linear-least-squares fits. Figure 8 shows that the deviations of the measurement results from the model are well within our error bars. In other words we conclude that the grating functions similar to what we expect in the sense of the angular pattern in the level of accuracy we can achieve.
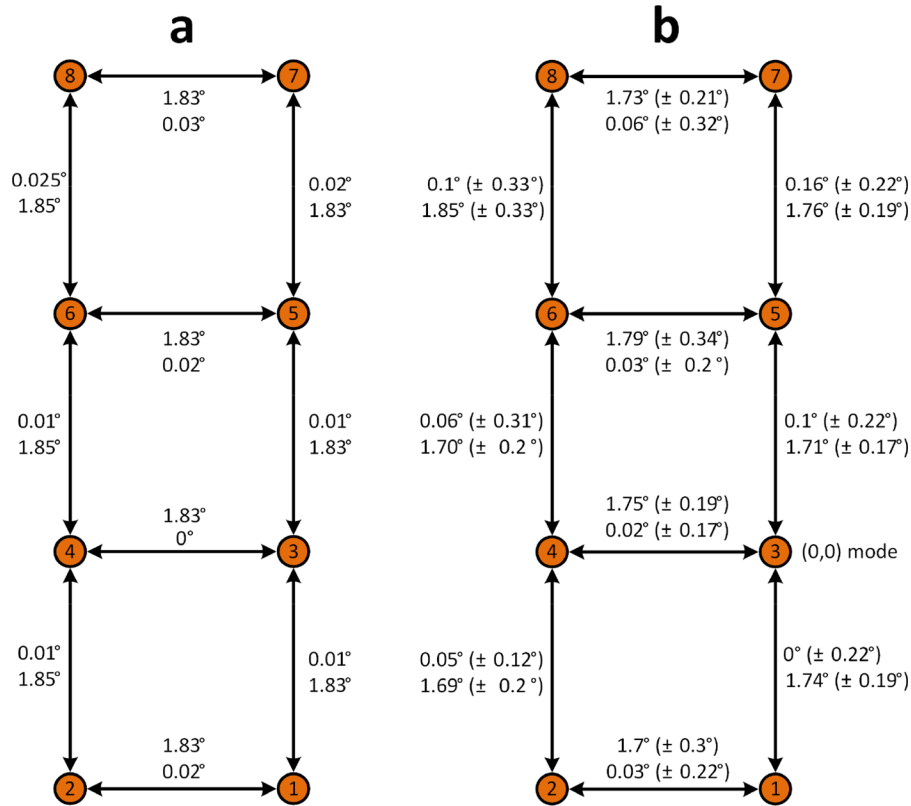
Fig. 8. The expected (a) and measured (b) angular distances between the beams. The top and bottom numbers on the arrows are the horizontal and vertical distances between its two end beams respectively. In prentices are the total uncertainties caused as explained in the text.

To be able to find the grating efficiency and power distribution uniformity we further open the aperture 2 and move the grating closer to it (∼ 10 cm away). In this way we are able to scan the diffracted beams close to their wastes, where they are smaller and better separated. This decreases the chance of interference with the side-lobes of the adjacent beams as well. Moreover, we shorten the optical path and increase the signal-to-noise ratio. We scan the beams at ∼ 34 cm after the grating with a pattern shown in Fig. 9(a), where the (0,0) order mode is indicated. The Fig. 9(b) is the incident beam scanned on the same plane when the grating is replaced with a flat mirror. We find this pattern reasonable, in which the incoming beam is nearly duplicated to the diffracted beams with little differences, which are attributed again to the contribution of the side-lobes.

To derive the power distribution we do the integration of the intensity for each measured beam. Figure 10 shows the (normalized) measured intensity for each beam at the QCL frequency together with what is expected form modelling at both the QCL frequency and the target frequency, for
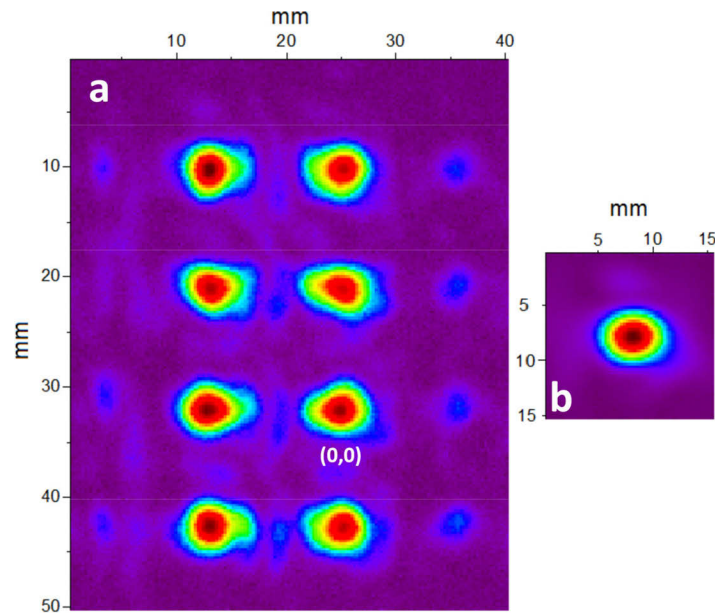
Fig. 9. (a) The scanned output beam pattern. (b) The incident beam scanned in the same plane when the grating is replaced with a flat mirror

which the grating is designed. Although these plots do not fully follow each other they still show similar non-uniformity levels of ∼ 13%. The lack of the one-to-one matching can be attributed to a couple of factors e.g. manufacturing imperfections and measurement uncertainties. We also looked at the possible effect of the different angles of each beam with respect to the scanning plane (the detector) on the derived integrated power. To do so, in a separate experiment we compare the integrated intensities of a beam in two cases, when it is perpendicular to the scanning plane and when it has a 4 ° angle, where we find a negligible difference. 4 ° is larger than the maximum difference in the angle to the scanning plane between the beams i.e. 2×1.83 °.

We derive an efficiency of 69% with an uncertainty of about ± 5% by taking the ratio between the sum of the integrated intensities of the main output beams and the one for the input beam scanned at the same plane as the output after replacing the grating with a flat mirror. This is the same efficiency as we expect from modelling. The uncertainty is due to the fact that the main output beams and the higher order modes are not well separated, which generates errors in defining the right integration area.

Having achieved important measurement results i.e. the angular pointing of the output beams, the efficiency, and the power uniformity to be in a good agreement with those from the design, our phase grating meets the requirements of GUSTO.
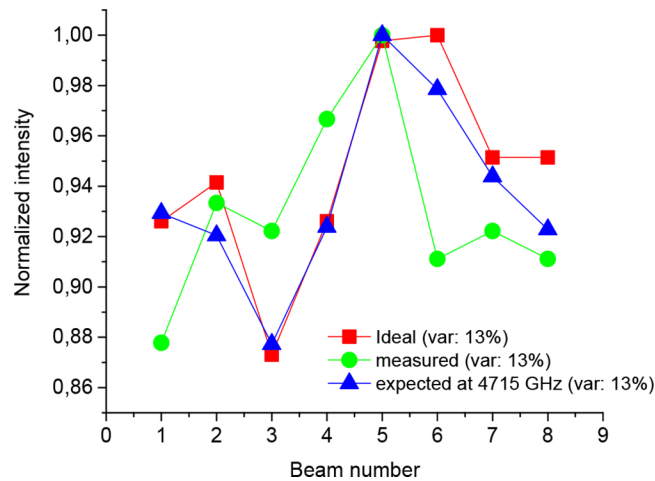
Fig. 10. The intensity distribution among the beams, which are numbered similar to Fig. 8. Three curves are plotted for the modelling results at the design (4.745 THz) and measurement (4.715 THz) frequencies, and for the measurement results. The distribution variations are noted in the figure.

5. Conclusions

We present a 4.7 THz asymmetric-profile Fourier phase grating for GUSTO as a 1 to 8 LO multiplexer. We designed, manufactured and experimentally tested this device. We have characterized the power distribution and efficiency at 4.7 THz using a quantum cascade laser as the input source. In particular, we characterize the angular distribution of 8 diffracted beams, where we find it following our design values within our measurement uncertainty of below 0.4 °. Such angular characterization with so high accuracy has never been reported before for these devices. Furthermore, the surface tolerance and its effects on the output beams uniformity and consequently the array sensitivity are also studied. We believe that this is the first demonstration of an asymmetric grating at a THz frequency. The presented phase grating that meets the criteria is now successfully integrated in the band-3 array receiver of GUSTO, which is scheduled to launch in December 2021 from Antarctica.

Disclosures. The authors declare no conflicts of interest.

Data availability. Data underlying the results presented in this paper are not publicly available at this time but may be obtained from the authors upon reasonable request.

References

1. J. V. Siles, R. H. Lin, C. Lee, E. Schlecht, A. Maestrini, P. Bruneau, A. Peralta, J. Kloosterman, J. Kawamura, and I. Mehdi, "Development of high-power multi-pixel LO sources at 1.47 THz and 1.9 THz for astrophysics: present and future," in *Proceedings of the 26th International Symposium on Space Terahertz Technology* (Cambridge, MA, 2015), pp. 40–42.
2. B. S. Williams, "Terahertz quantum-cascade lasers," Nat. Photonics **1**(9), 517–525 (2007).
3. B. S. Williams, H. Callebaut, S. Kumar, Q. Hu, and J. L. Reno, "3.4-THz quantum cascade laser based on longitudinal-optical-phonon scattering for depopulation," Appl. Phys. Lett. **82**(7), 1015–1017 (2003).
4. T.-Y. Kao, Q. Hu, and J. L. Reno, "Perfectly phase-matched third-order distributed feedback terahertz quantum-cascade lasers," Opt. Lett. **37**(11), 2070–2072 (2012).

5. A. Khalatpour, J. L. Reno, N. P. Kherani, and Q. Hu, "Unidirectional photonic wire laser," Nat. Photonics **11**(9), 555–559 (2017).

6. B. Mirzaei, J. R. G. Silva, D. Hayton, C. Groppi, T. Y. Kao, Q. Hu, J. L. Reno, and J. R. Gao, "8-beam local oscillator array at 4.7 THz generated by a phase grating and a quantum cascade laser," Opt. Express **25**(24), 29587–29596 (2017).

7. B. Mirzaei, Y. Gan, J. R. Silva, M. Finkel, S. Yates, W. Laauwen, A. Young, C. Walker, and J. R. Gao, "Asymmetric phase grating as 4.7 THz beam multiplexer for GUSTO," in *Proceedings of the 30th International Symposium on Space Terahertz Technology* (Gothenburg, Sweden, 2019), pp. 114–116.

8. B. Mirzaei, J. R. G. Silva, Y. C. Luo, X. X. Liu, L. Wei, D. J. Hayton, J. R. Gao, and C. Groppi, "Efficiency of multi-beam Fourier phase gratings at 1.4 THz," Opt. Express **25**(6), 6581–6588 (2017).

9. U. U. Graf and S. Heyminck, "Fourier gratings as submillimeter beam splitters," IEEE Trans. Antennas Propag. **49**(4), 542–546 (2001).

10. Y. Gan, B. Mirzaei, J. R. G. Silva, A. Khalatpour, Q. Hu, C. Groppi, J. V. Siles, F. van der Tak, and J. R. Gao, "81 supra-THz beams generated by a Fourier grating and a quantum cascade laser," Opt. Express **27**(23), 34192–34203 (2019).

11. W. Zhang, P. Khosropanah, J. R. Gao, T. Bansal, T. M. Klapwijk, W. Miao, and S. C. Shi, "Noise temperature and beam pattern of an NbN hot electron bolometer mixer at 5.25 THz," J. Appl. Phys. **108**(9), 093102 (2010).